2018

Spectroscopic study of excited molecular nitrogen generation due to interactions of metastable noble gas atoms

Laurence Scally

James Lalor

Miroslav Gulan

See next page for additional authors

Authors

Laurence Scally, James Lalor, Miroslav Gulan, Patrick J. Cullen, and Vladimir Milosavljevic

FULL PAPER

Spectroscopic study of excited molecular nitrogen generation due to interactions of metastable noble gas atoms

Laurence Scally[1] (ID) | **James Lalor[1,2]** | **Miroslav Gulan[1]** | **Patrick J. Cullen[1,3]** (ID) | **Vladimir Milosavljević[1,4]** (ID)

[1] Bioplasma Research Group, Dublin Institute of Technology, Sackville Place, Dublin 1, Ireland

[2] School of Applied Technology, Dublin Institute of Technology, Bolton Street, Dublin 1, Ireland

[3] Department of Chemical and Environmental Engineering, University of Nottingham, Nottingham, NG7 2RD 2, UK

[4] Faculty of Physics, University of Belgrade, P.O.B. 368, Belgrade 11000, Serbia

Correspondence
Laurence Scally, Bioplasma Research Group, Dublin Institute of Technology, Sackville Place, Dublin 1, Ireland.
Email: laurence.scally@dit.ie

Funding information
Science Foundation Ireland (SFI), Grant number: 14/IA/2626

This work provides an insight into the generation of excited nitrogen species by allowing noble gases to interact both with one another and ambient air. He and Ar were utilized to generate the optimum selectivity process to create reactive nitrogen species. An optimum setting for the generation of excited molecular nitrogen species, based on their excited energy levels, was obtained when using a mixture of Ar-He at a ratio of 10:1. At that point, when a voltage of 27 kV is applied to the system, it reached the maximum efficiency for selectivity processes to occur which allowed for a greater non-radiative transfer of energy through the mixture of noble gas atoms and into the molecular nitrogen present in ambient air.
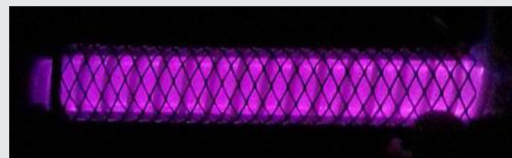
KEYWORDS

AC barrier discharges, kinetics, nitrogen, non-thermal plasma, optical emission spectroscopy (OES)

1 | INTRODUCTION

Non-thermal plasma (NTP) discharge in open air results in charged species, energetic photons, active radicals, and also a low degree of ionization gas.[1,2] Measurements and analysis of the physical and chemical interactions of NTPs has been a subject of intense study for many decades. Optical spectroscopy may, however, provide better insights into the reactive species being generated, the electron energy range within the plasma for atomic and molecular excitation, and the mechanisms and kinetics of energy transfer with respect to radiative and collisional processes.[3–7] Through this, the possible chemical reactions that could interact with surfaces can be ascertained. With this in mind, NTPs have gained a lot of attention for potential applications ranging from agriculture to medicine.[8–11] Plasma interaction with sample surfaces can cause surface modification, functionalization, sputtering, and etching. Examples include atomic etching of circuits or deposition of oxygen species onto polymers.[12–14] Furthermore, when used on organic samples, the introduction of oxygen or nitrogen containing radicals can sterilize surfaces due to an increase of reactive oxygen and nitrogen species that cause stresses within organic matter, which leads to degeneration. These processes can inactivate the likes of *Escherichia coli*.[15,16]

Many treatments utilize molecular nitrogen (N_2) as a working gas.[17–22] Ambient air introduces the N_2 species into the system used in this work to interact with the other gases used. As well as introducing N_2, the ambient air present in the system brings with it a certain amount of humidity and thus adsorbed moisture content, which can give rise to the formation of hydroxyl radicals (OH) and atomic hydrogen (H) when plasma is ignited in the system. There are, however, other species that are produced from sources such as factories

and vehicles which include nitrous oxides (NO_x) and other greenhouse gases which are considered to be hazardous emissions. By utilizing NTP systems, it has been shown that hazardous pollutants such as NO_x can be broken down into much more acceptable species that are not as harmful as the hazardous waste and volatile organic compounds that are the byproduct of many industrial and mechanical processes.[23,24] The implementation of NTP systems is not restricted to industrial processes. They have seen a growing use in material processing, nanotechnology, and medical applications.[25,26] An added benefit to atmospheric plasma chemistry is that they can be used to destroy bacterial cells and other organic materials growing on surfaces which one would want to sterilize.[27–30] In order to understand the formation of the many reactive nitrogen species (RNS) and reactive oxygen species (ROS) that can be produced, the gas chemistry and kinetics of a system must be analyzed thoroughly.

The second positive system (SPS) of the excited N_2 emission bands are seen in the near-UV region. The emission wavelengths range from 315 to 450 nm and the specific peaks of interest in this work are at 315, 337, 357, 380, 405, and 425 nm with an emission of ionic nitrogen (N_2^+) from the first positive system (FNS) at 391 nm. The emission from the SPS are due to transitions from $C^3\Pi_u \rightarrow B^3\Pi_g$ and the emissions of the FNS system are due to transitions from $B^2\sum_u^+ \rightarrow X^2\sum_g^+$. Argon (Ar) and helium (He) were chosen as a means of increasing nitrogen production under optimum control parameters (e.g., lower voltages compared to ambient air alone) as they are known to aid in the production of the excited N_2 species. By determining a correlation between the emissions of these species, it can be shown that absolute emission intensities can be used as an indicator to benchmark the most efficient conditions for generation of the excited nitrogen species. In this work an atmospheric plasma system, which operates with noble gas and ambient air chemistry, was employed. The system operates at a frequency of 50 kHz and makes use of a cylindrical dielectric barrier discharge geometry with a helically inclined dielectric barrier. He and Ar were used individually with permeating ambient air as a background gas to develop a baseline of nitrogen emissions. After determining the interactions that occur between Ar and He with ambient air present within the system, they were then mixed at different ratios as a means to show a selectivity process to optimize the generation of excited nitrogen species. The resonant and metastable atoms of Ar and He are taken into consideration when determining the possible pathways and mechanisms of energy transfer for excited nitrogen generation. Studying the impact of He and Ar on N_2 generation of the SPS and FNS and how to optimize it was the main goal of this experiment. The experiment aims to provide a better understanding of (i) the chemistry and physics of noble gases with ambient air; (ii) how to create an environment

which can either increase excited N_2 species or reduce the possible interactions of energetic Ar and He with samples sensitive to etching or atomic bombardment (i.e., utilizing a method that optimizes nitrogen excitation through selectivity processes); and (3) how to do so without generating NO_x and other greenhouse gases.

2 | EXPERIMENTAL

2.1 | Experimental setup and electrical diagnostics

The device used to carry out the OES measurements in this work was an Edmund Optics CCD spectrometer. Due to the resolution of this device being in a range of 0.6–1.8 nm (wavelength dependent), some emission peaks overlapped and could not be fully analyzed with confidence. Spectral emissions could be recorded between 200 and 850 nm. The spectra were recorded through BWSpec™ software and analyzed by integrating the area under each peak. By implementing OES, it could be found how certain parameters change the interactions within the plasma and ascertain which parameter had the highest impact on the plasma kinetics and characteristics. The flow rates of the gases were varied from 1 to 5 L min^{-1} when using each gas individually. When mixing
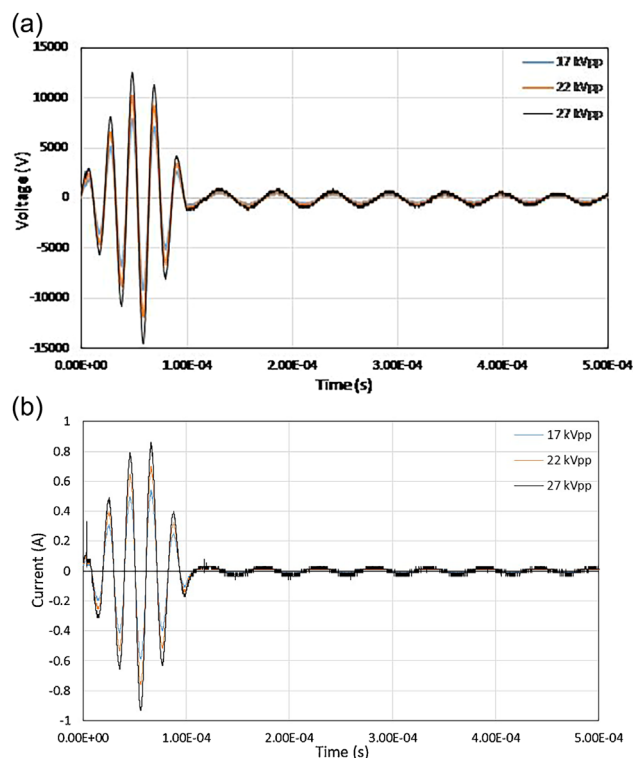

FIGURE 1 a) Reading of maximum voltage waveforms when frequency was set to kHz and the voltage applied was 17, 22, and 27 kV. (b) Discharge current waveform recorded when using the three listed voltages

the gases, ratios from 10/1 to 2/1 were used. This was achieved by keeping one gas at a constant flow rate of $1 \, \text{L min}^{-1}$ and varying the other from 0.1 to 0.5 L min^{-1}. Prior to inducing the plasma discharge, the gases were allowed to flow through the system to flush the reactor so as to equalize the emissions obtained and minimize any fluctuations over time. The frequency used was 50 kHz. This was found to be the resonant frequency that gave the optimum plasma discharge within the system. Going above or below this resulted in lessening reduction of the emission intensities and changing the frequency by ±1.5 kHz resulted in cessation of the plasma discharge. The optimum frequency was chosen through the use of OES monitoring and obtaining the maximum values from the voltage and discharge current waveforms for 17, 22, and 27 kV. These can be seen in Figure 1.

Overall there were 15 points of measurement; five positions along the length of the system with three different sides (top, left, and right). The length of the aluminum ground electrode was 190 mm long and the outer radius of polycarbonate tube was 16 mm. The discharge gap between the dielectric surface and the inner radius of the polycarbonate tube was 8 mm. The HV steel axle had a radius of 5 mm, the inner radius of the polycarbonate tube was 14 mm and the dielectric thickness is 1 mm. The material used to make up the helical dielectric barrier was acetal. The setup of the system is shown in Figure 2.

2.2 | Analysis of spectral lines

The OES data that was recorded during the experimental procedure described in this work was analyzed using an integration process. The peak associated with the wavelength of each species was documented and the absolute value was found by setting a minimum and maximum for each emission. This was then integrated to give the total counts for each species to give a singular value, which was divided by a factor of 1×10^3 in order to create an easier comparison between results. When obtaining the data for the emission spectra of the plasma discharge, a temporal evolution analysis of the discharge was carried out by acquiring 21 spectra for each measurement. This was done by measuring the emission intensities every 5 s with an integration time of 750 ms for a total of 100 s, with the first spectra being recorded at the zeroth moment. These spectra were then analyzed through integration of the peaks as described above. However, in order to calculate the error of the averaged values, the standard deviation was calculated by using each intensity that was measured during the 100 s measurement timeframe as the comparison value against the mean value plotted. After obtaining the standard deviation the standard error was calculated for each mean value.
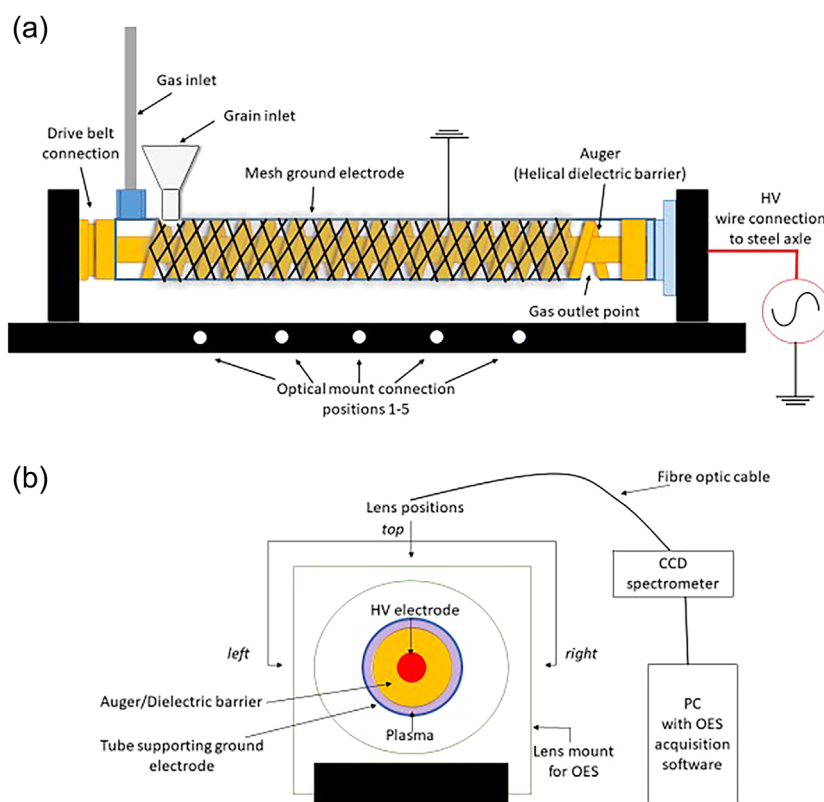

FIGURE 2 a) Diagram of plasma system setup which can treat samples internally between the auger flights where plasma discharge is created. b) Optical mount setup for OES measurements

2.3 | Spectral information for species generated with ambient air

Plasma systems that are exposed to ambient air, whether it is an unsealed dielectric barrier discharge system or a plasma jet that injects plasma into open air, there are certain factors to take into consideration. These include the changes in humidity, ventilation speed, and impurities introduced by the air. Humidity aids in the creation of emission lines of hydroxyl radicals (OH), hydrogen (H), nitrous oxides (NO_x), atomic oxygen (O), and excited molecular nitrogen of the SPS and FNS (N_2 and N_2^+). Measurements using OES show that, for this study, there seems be no emission lines for NO or O. Importantly, there was a clear detection of the SPS and FNS of N_2 from 315 to 425 nm. These emission bands were of highest interest in order to compare the dynamic relationship between Ar metastables and high energy atomic He.

The spectral emissions of the SPS have an excited energy range of 11–11.2 eV and the N_2^+ emission of the FNS at 391 nm has a threshold energy of 18.8 eV. High energy electrons and/or He metastable species can contribute sufficient energy to ionize molecular nitrogen and generate the emission seen at 391 nm. However, the SPS emissions seen can be created through the direct excitation of neutrals from low energy electrons. The SPS emission lines have similar excitation energies, but their emissions occur at different wavelengths due to their energy levels after emission being different. For example, those at $\lambda = 337, 357, 380$, and 405 nm all have an excited vibrational quantum number of $v' = 0$ (in the $C^3\Pi_u$ state), but their quantum vibrational numbers after emission are $v'' = 0, 1, 2, 3, \ldots 12$ (in the $B^3\Pi_g$ state). This gives rise to the spread of emission throughout the band and a main peak ($v = 0 - v'' = 0$) among the band heads (namely $\lambda = 337$ nm for the SPS and $\lambda = 391$ nm for the FNS). Species that are also observed in this work are the emissions of OH and H. The dissociation of H_2O is the main cause of OH and H. The details of all the species related to the presence of atmospheric air seen in the OES measurements are shown in Table 1.

TABLE 1 Spectroscopic data used for species generated with the presence of ambient air [31–33]

Excitation energy (eV)	Emission wavelength (nm)
4.17	OH-310
11.20	N_2-315
11.01	N_2-337
11.01	N_2-357
11.01	N_2-380
18.8	N_2^+-391
11.01	N_2-405
11.20	N_2-425
12.09	H_α-656

2.4 | Spectral information for Ar

Many plasma systems use Ar as an operating gas due to its inert nature and steady state discharge.[34] The applications that utilize Ar the most are those that require some form of etching, bombardment, or other physical interaction which will not oxidize surfaces.[35] Examples of such uses and processes include the cleaning of metallic surfaces, etching of circuit boards, and ablation of solid/powder samples.[36,37] However, these processes are usually performed within a vacuum chamber so as to eliminate any cross contamination. Therefore, when used in open air there are some extra considerations to keep in mind. Although Ar itself is chemically inert, it has sufficient energy to aid in the generation of reactive species through interaction with atoms and molecules present in the ambient air. An example of this is the dual effect of etching and functionalization that can be induced on polymer surfaces through the use of Ar-air plasmas. As Ar bombards the surface and creates atomic crevices, atomic oxygen or OH can bind to free bonds on the surface to create a more hydrophilic environment. This work focuses on those interactions by allowing the Ar to flow through a system that has ambient atmospheric air residing inside of it and accessing it throughout the experiment from various opening points.

By using Ar as the main working gas, the breakdown voltage of the system drops to less than half of what is necessary when using solely ambient air, for example, ambient air required at least 40 kV peak to peak (PP) to observe any plasma discharge and Ar began at 13–14 kV (PP). Creating a lower threshold for plasma discharge is because Ar allows for a build-up of excited species and energetic particles, such as electrons, whereas air quenches this affect due to the strong electronegativity of oxygen. The main point of interest for this study is how this introduction allows for the generation of selected excited nitrogen species. By utilizing the metastables created when generating a plasma discharge with Ar, N_2 can be excited through non-radiative energy transfer. The atomic species used in this study can be seen in Table 2, with the emissions arising from the de-excitation branching of Ar metastables denoted by $1s_5$ and $1s_3$ in Paschen notation.[38] The other emission wavelengths are associated with excited Ar atoms that have their promoted electron situated in a resonant state.

The Ar-750 atomic emission line is sensitive to the high-energy electron region of the electron energy distribution function (EEDF) and is created through direct excitation from high-energy electrons. Conversely, the Ar-811 atomic emission line is sensitive to low-energy electrons. By using a line ratio method, the distribution of high and low energy electrons can be ascertained, providing insights into how the reaction mechanisms and gas kinetics occur. The EEDF for

TABLE 2 Spectroscopic data of Ar used for this study[29]

Excitation energy (eV)	Wavelength (nm)	Paschen notation
13.33	Ar-696	$2p_2 \rightarrow 1s_5$
13.33	Ar-727	$2p_2 \rightarrow 1s_4$
13.48	Ar-750	$2p_1 \rightarrow 1s_2$
13.17	Ar-763	$2p_6 \rightarrow 1s_5$
13.15	Ar-772	$2p_7 \rightarrow 1s_5$
13.28	Ar-794	$2p_4 \rightarrow 1s_3$
13.09	Ar-801	$2p_8 \rightarrow 1s_5$
13.08	Ar-811	$2p_9 \rightarrow 1s_5$
13.33	Ar-826	$2p_2 \rightarrow 1s_2$

plasma that use Ar can be obtained by using the line ratio of Ar-811/Ar-750.[39] The main transitions of interest for calculating the EEDF are the radiative decays of Ar-750 ($2p_1 \rightarrow 1s_5$) and Ar-811 ($2p_9 \rightarrow 1s_5$). The $2p_1$ line is dominated by direct excitation from the ground state by high energy electrons, whereas the $2p_9$ is reported to be dominated by excitations from low energy electron interactions. The possible pathways that the Ar 2p levels may be populated through include direct excitation from the ground state, excitation of 1s metastables from low energy electrons, and cascade excitation from upper levels such as ($3p^5 5s$ and $\rightarrow 3p^5 5d$ levels). The metastable levels accessible to create the 2p levels are $1s_3$ and $1s_5$ since the resonant states ($1s_2$ and $1s_4$ rapidly decay to the ground state) $1s_5$ has been found to have a much larger direct excitation cross-section between the two.[40–42] The peak cross-section has consistently been found to be much larger for the $1s_5$ excitation to the $2p_9$ level than for the excitation cross-section for the ground state, with values being 15–700 times higher for the $1s_5$ level.[42] Due to the forbidden and allowed states and the dipole/parity rules, the dominant transitions that allow for the population of $2p_9$ is from the metastable $1s_5$ state from low energy electron interactions, while the population of $2s_1$ is generated by direct excitation from the ground state due to high energy electrons.[43] From this, it can be ascertained that a ratio of ($2p_9 \rightarrow 1s_5/2p_1 \rightarrow 1s_2$) (Ar-811/Ar-750) gives a ratio of low energy electron to high energy electron excitations.

2.5 | Spectral information for He

The emission spectra recorded during this study revealed four emission lines of He. These emission lines can be subdivided into two different categories of energy sets: singlet and triplet. Transitions of electrons between singlet and triplet states are forbidden due to dipole–dipole interactions and the breaking of symmetry of electron configurations and spin reversals. Electrons may only pass from a singlet state to a triplet state, or vice versa, through non-radiative processes known as intercombination crossing. However, these crossings have very low transition probabilities for neutral He. Due to this, only emissions from these energy sets are analyzed in this work rather than their interactions with one another. The singlet states of atomic He analyzed are He-667 and He-728 with the triplet states being He-587 and He-706.

The metastables that He can produce have high energy levels and allow for non-radiative transfer of energy to N_2 with sufficient energy to create excited N_2 of the SPS and FNS. The atomic He emissions at He-471, He-587, He-667, He-706, and He-728 have energy levels that are the same as the resonate levels of their respective energy sets. To further determine the kinetics within the plasma discharge the EEDF was calculated for the He discharge using the line ratio method as for Ar. However, the lines used when carrying out the calculation for He were: N_2-337 and N_2^+-391. N_2-337 is sensitive to changes caused by low energy electron, and N_2^+-391 is sensitive to changes from high energy electrons. Given the high energies of excited He and the long lived metastable species that can be generated, it is often put forward that these species are responsible for the formation of N_2^+-391. However, in some studies it has been argued that electron collisions are the most dominant and influential particles in the formation of N_2^+-391. Works have been carried out that bring forward the point that the difference in excitation cross-sections between He atoms and N_2. The smaller cross-section of He compared to N_2 allows free electrons to have more time to be accelerated by the applied electric field and are thus able to reach higher energy levels that can ionize N_2 and generate N_2^+.[44] Another work that uses a He gas flow in a plasma jet that shows the interactions and kinetics with ambient air, a steady state reaction process is considered along with the dominance of electron impact excitation of N_2 to N_2^+-391.[45] The work carried out by Begum et al. used the ratio of the excited N_2 species from the SPS and FNS to show how the electric field changes and how the electron kinetics vary with different percentages of air to He. So from this, we assume, much like the work they carried out, that the dominant process for N_2^+-391 generation is due to high energy electron collision with N_2 due to the lower cross-section value of He allowing the free electrons to be accelerated by the applied electric field. Getting a ratio of N_2-337/N_2^+-391 gives the ratio of low energy electrons to that of high energy electrons with values >1 meaning a larger population of slow electrons and <1 equating to a larger population of fast electrons.[46] Information used for the identification and analysis of the emission species of He that were used in this work are seen in Table 3.

TABLE 3 Spectroscopic data of He used for this study[29]

Excitation energy (eV)	Wavelength (nm)
23.59	He-471
23.07	He-587
23.07	He-667
22.72	He-706
22.92	He-728

3 | RESULTS

Due to the cylindrical geometry of the system used in this experiment, it was assumed that the plasma generated would be homogenous throughout. Analyzing the data from the OES measurements showed that this is the case. When comparing the results from point to point, the same ratios and emission patterns were observed, thus highlighting the strength of the method of analysis when comparing the emission intensities relative to one another. Changes in the flow rate of the gases did affect the emission of certain species. However, the emissions changed linearly with increasing flow rates and remained stable over time. The greatest changes occurred due to increases in the applied voltage. In order to summarize the results into concise graphs, the emissions from the plasma that were recorded when using the lowest and highest flow rates at each of the three voltages (17, 22, and 27 kV PP) for each gas were analyzed. Due to the homogeneity of the plasma, the results shown were taken from the top of the first position as a representation of the whole geometry.

3.1 | Discharge of Ar in ambient air

The plasma generated when using Ar showed strong emissions of Ar, OH, and N_2 (SPS). There were also small, but distinguishable emissions of H_α at 656 nm. As seen in Figure 3 the intensities of N_2 increases with the use of higher voltages, but they also decrease with an increase in flow rate. However, the intensities of the excited Ar species increase with both voltage and flow rate. When the flow rate of Ar is increased, the ambient air within the system is flushed out even more so and the quantity Ar being introduced increases. In this case the percentage of Ar is higher and more excited atomic Ar emissions can be measured, whereas in the case of ambient air there is a decrease of N_2 and OH with an increase of the Ar flow rate. From the analysis of the emission intensities as shown in Figure 3(a,b), it can be observed that the atomic Ar species and excited N_2 species of the SPS have interactions with one another. The kinetic mechanisms
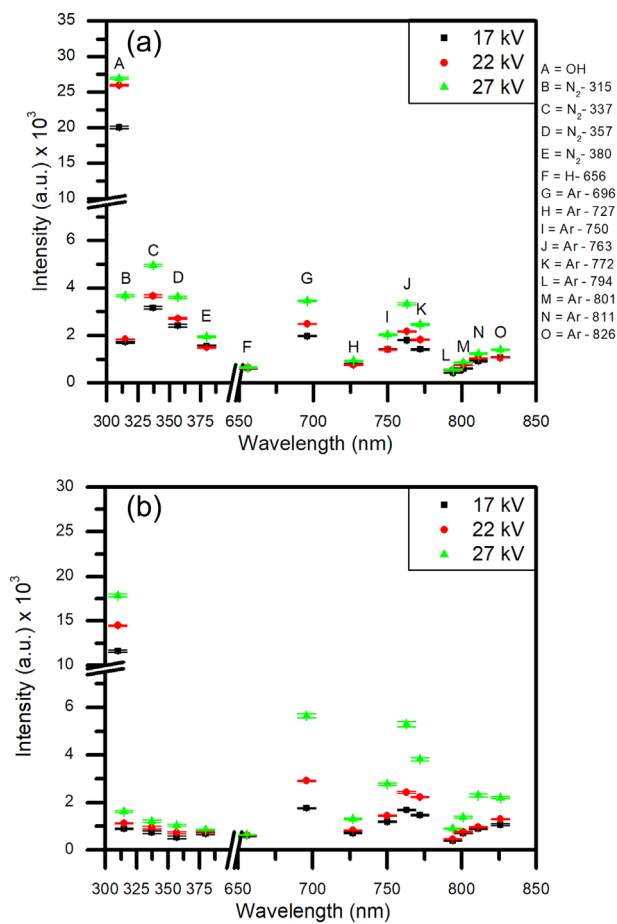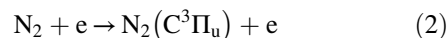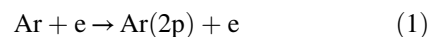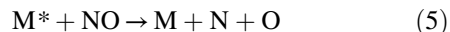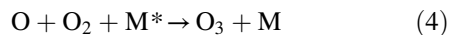

FIGURE 3 The changes in the intensities for the N_2 SPS, OH, Ar, and H_α are shown with the species being represented by their wavelength on the x-axis. The legend in (a) labels the species (A–O) for each wavelength displayed. a) Shows the intensities when the flow rate of Ar is kept at $1\,L\,min^{-1}$ and (b) represents intensities when the Ar flow rate is $5\,L\,min^{-1}$

(1–3) show the interactions that are most probable to generate excited Ar and N_2 species.[41] Mechanisms (4–7) show how O and NO are destroyed and are not detected within this plasma discharge.[41] The intensity of the emissions that occur due to the relaxation of the Ar metastable species increase with voltage and gas flow rate, but not as much when compared to that of Ar-727 and Ar-826. As the metastables of Ar are known to transfer energy to N_2 to generate the SPS system, it is expected that these excited Ar species would not increase as much compared to their resonant state due to their greater ease of being quenched.

$$Ar + e \rightarrow Ar(2p) + e \qquad (1)$$

$$N_2 + e \rightarrow N_2\left(C^3\Pi_u\right) + e \qquad (2)$$

$$Ar(2p) + N_2 \rightarrow Ar + N_2\left(C^3\Pi_u\right) \quad (3)$$

As can be seen from the data presented, there is no detection of NO or O in the emission spectra obtained. The lack of these species can be explained by the assertion of mechanisms (4–7) below where M is a third body atom or molecule.[47] In this experiment, M is considered to be Ar or He.

$$O + O_2 + M^* \rightarrow O_3 + M \quad (4)$$

$$M^* + NO \rightarrow M + N + O \quad (5)$$

$$O + H_2O \rightarrow 2OH \quad (6)$$

$$2N + M \rightarrow N_2 + M \quad (7)$$

The intensity of Ar-750 does change noticeably with a change in voltage, but does vary with a change in flow rate. The excitation of Ar-750 is due to the impact of high energy electrons so it is an indicator of how the distribution of electron energies change with the parameters used. This is shown in Figure 4 which were obtained by using the line ratio method Ar-811/Ar-750 giving the EEDF. The increases of EEDF can be caused by a larger concentration of Ar being present at higher flow rates, which allows for more kinetic interactions in the form of electron-Ar collisions which are not quenched as much through energy transfers processes with N_2.
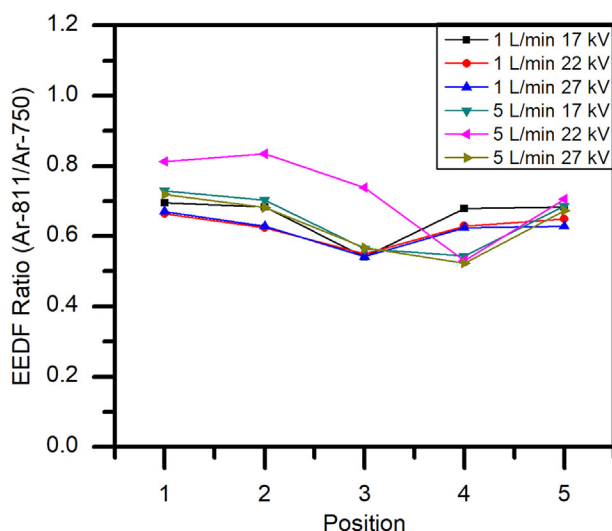

FIGURE 4 The changes in the averaged EEDF across five positions along the plasma discharge system, obtained from the line ratio of Ar-811/Ar-750 when using Ar at a flow rate of Ar = $1\,L\,min^{-1}$ and Ar = $5\,L\,min^{-1}$
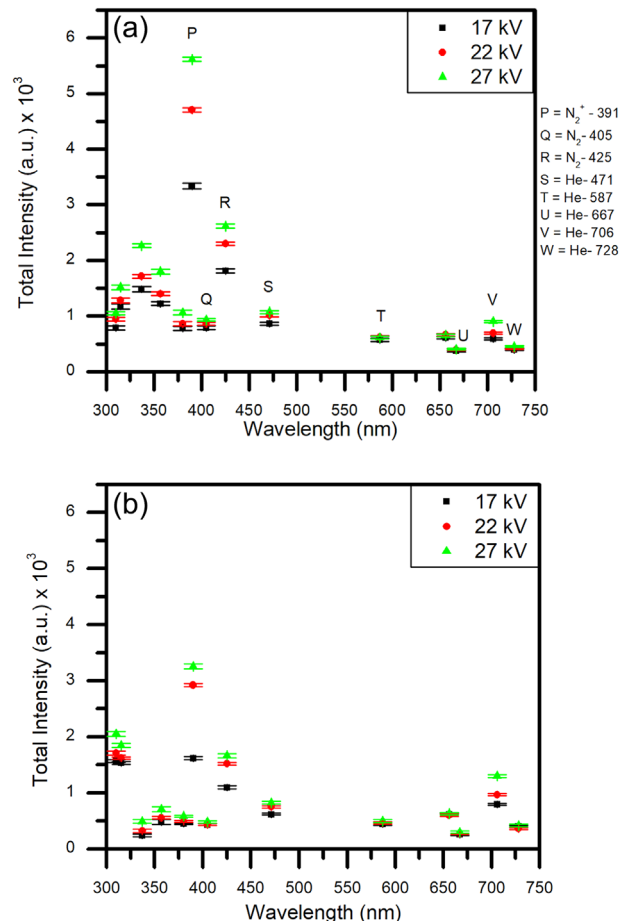

FIGURE 5 The changes in the intensities for OH, N_2, N_2^+, H_α, and He are shown with the species being represented by their wavelength on the x-axis. The legends in 3(a) label species (A-E) and 5(a) labels the species for every other wavelength displayed on (a and b). a) Shows the intensities when the flow rate of He is kept at $1\,L\,min^{-1}$ and (b) represents intensities when the He flow rate is $5\,L\,min^{-1}$

3.2 | Discharge of He in ambient air

Figure 5(a,b) show the dependence of the emissions of N_2 from the SPS and FNS with respect to changes in voltage and gas flow rate. They also show the dependence of He emissions on voltage and gas flow rate. The trends seen for N_2 are the same as when Ar was the operating gas. However, there is an increase in the number of excited N_2 species generated in the SPS and there is also N_2^+ generated from the FNS at 391 nm. The intensity of He undergoes noticeable changes with changes in voltage and flow rate. An increase in voltage increases the excited population density of He, but an increase in gas flow causes a decrease in two of the atomic He species (He-471 and He-587) at 23.0736 and 23.59 eV and increase in one atomic He species (He-706) at 22.72 eV. Compared to the use of Ar as the main feed gas, the increase of the He flow rate through the system shows an increase in the emission of OH. The changes in

emissions of N_2^+ and He when comparing the flow rate of 1–5 L min^{-1} suggest that the increased flow rate introduces more He and reduces the amount of ambient air in the system and does not quench the excited He species as much. This in turn allows for the energetic He species to interact with the H$_2$O adsorbed within the system more so and generated more OH. The kinetic mechanisms (8–10) as well as mechanisms (1–7) highlight the most probable routes for energy transfer and generation of the species seen in the emission spectra.[48]

$$He + e \rightarrow He(2S_3) + e \quad (8)$$

$$He + e \rightarrow He^+ + 2e \quad (9)$$

$$N_2 + e \rightarrow N_2^+ + 2e \quad (10)$$
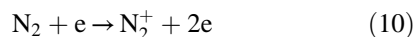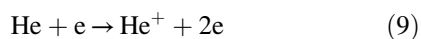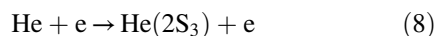
The EEDF for He plasma was calculated from the line ratio method with the emission lines of N$_2$-337 and N$_2^+$-391 and is shown in Figure 6. The shown EEDF values were found when the flow rate was set to 1 and 5 L min^{-1} and for all three voltages used (17, 22, and 27 kV PP). The somewhat more spontaneous changes in the EEDF compared to the other gases and gas mixes is that excited N$_2$ densities would be higher at the beginning of the system and become saturated until they reach another point further down the system, but with higher flow rates, they become more dispersed throughout the system. The generation of He* and He$^+$ within the plasma would give rise to high energy species and electrons. So the increase of these species would not impact the generation of N$_2^+$ at 391 nm as much as N$_2$ in the SPS.
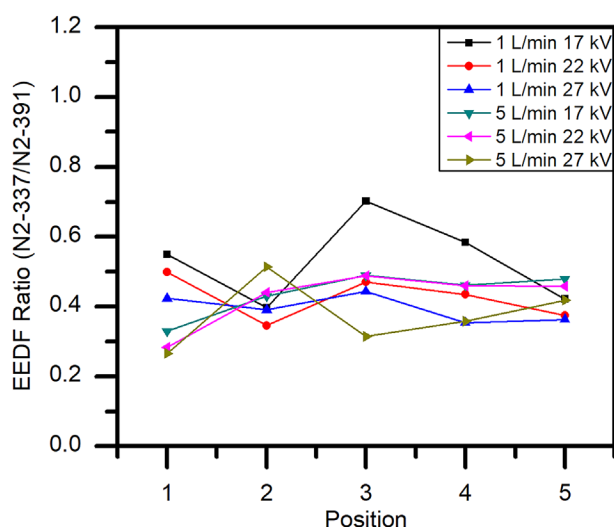
3.3 | Discharge of an Ar-He gas mixture in ambient air

The use of Ar as the main carrier gas with the addition of He sees an increase in the generation of the N$_2$ SPS. Even though He is introduced into the system from 0.1 up to 0.5 L min^{-1} in intervals of 0.1 L min^{-1}, there are no noticeable emissions of the atomic He species or N$_2^+$ seen compared to when He was the only gas used to interact with the ambient air. With increases of voltage, all species other than H$_\alpha$ increase in intensity and this can be clearly observed from the trends shown for their respective intensities in Figure 7. However, it can also be seen in Figure 7 how the intensity of Ar is decreased with an increased addition of He into the gas mixture. By prescribing mechanisms (1–3 and 8–10) to the results found, the most probable kinetic mechanisms can be ascertained and show how the formation of N$_2$ is increased so
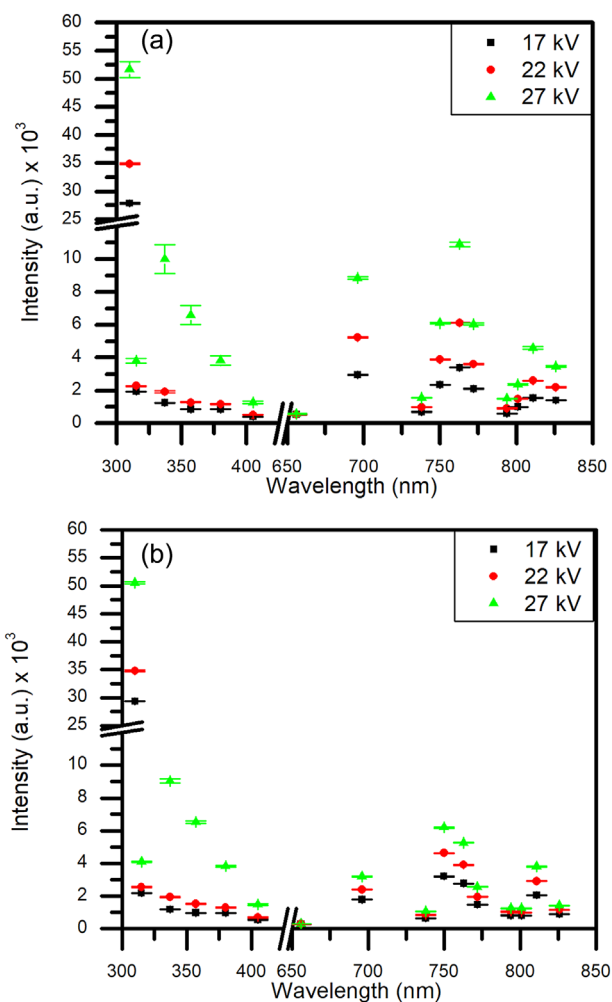
FIGURE 7 The changes in the intensities for OH, N$_2$, Ar, and H$_\alpha$ are shown with the species being represented by their wavelength on the x-axis. The legend in 3(a) labels species (A-O) and the legend in Figure 5(a) labels species (P) that can be seen here. Ar is kept at 1 L min^{-1} (a) shows the intensities when the flow rate of He is set to 0.1 L min^{-1} and (b) represents intensities when the He is set to 0.5 L min^{-1}

FIGURE 6 The changes in the average EEDF with respect to the positions along the plasma system, obtained from the line ratio of N$_2$-337/N$_2^+$-391 when using He in air when the flow rate was set to He = 1 L min^{-1} and He = 5 L min^{-1}

much while He or N_2^+ are not detected.[49,50] The quenching of He is most probable through Penning excitation or through lack of excitation due to its lower excitation cross-section compared to N_2.[44,49] Given that Ar emissions are at a maximum when He is set to $0.1 \, L \, min^{-1}$ and most of the Ar peaks drop when He is set to $0.5 \, L \, min^{-1}$, there must be some shift in the energy distribution as the Ar 750 line increases while the generation of N_2 SPS species stays relatively constant. Given that the Ar-750 line is associated with high energy electrons and that Ar acts as a quencher through Penning ionization, the increase of He takes away some of the population of excited Ar(2p) species through kinetic processes and creates an environment that allows for a higher generation of Ar-750. Given that N_2-337 is associated with low energy electrons and the SPS can be created by collisional processes with excited Ar species, the increase of the generation of Ar(2p) species compared to the plasma discharge when using only Ar with air gives rise to a higher population of excited species in the SPS. This can be seen in the process described by mechanism (11).

$$He^* + Ar \rightarrow He + Ar(2p) + e \qquad (11)$$
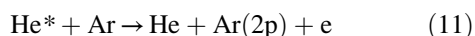
Since there is no detectable emission of N_2^+-391 when using a gas mixture of Ar-He, the EEDF must be calculated by using the same line ratio as was used for Ar. This shows that the quenching of He atoms through Penning excitation plays a significant role in the kinetics of Ar, and as a consequence, the generation of excited N_2 SPS and FNS species. Figure 8 shows the EEDF calculated for the gas mixture of Ar-He through the use of the same line ratio method employed for Ar as seen in Figure 4.
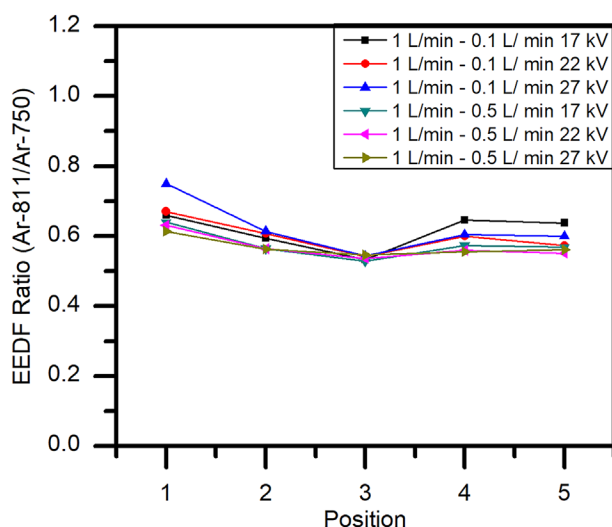

FIGURE 8 The changes in the average EEDF obtained from the line ratio of Ar-811/Ar-750 when using Ar-He in air are shown for five positions along the plasma system. Ar is kept at $1 \, L \, min^{-1}$ and the EEDF is shown for a flow rate of He $= 0.1 \, L \, min^{-1}$ and He $= 0.5 \, L \, min^{-1}$

3.4 | Discharge of a He-Ar gas mixture in ambient air

The introduction of Ar into the system when using He as the dominant gas creates a similar mix of species to the Ar-He mixture. However, there are slight differences in the values of the intensity. Interestingly, N_2^+ was not detected in the emission spectra even though the flow rate of He in this instance is at $1 \, L \, min^{-1}$, which has been shown to be sufficient to generate N_2^+ when only introducing He into the system. This means that the introduction of Ar, even at the lowest flow rate of $0.1 \, L \, min^{-1}$, is sufficient to quench the excited He species through Penning excitation and, therefore, impedes the generation of N_2^+ species. The intensity of N_2 species increases when the voltage is raised and is seen to decreases with an increase of Ar in the gas mixture. OH, however, has a higher intensity maximum when the amount of Ar in the gas mixture is greatest. This is clearly seen in Figure 9(a,b). The use of He with additives of Ar creates an environment in which the Ar-750 species have an increased intensity compared to a mix of Ar-He and even when Ar is used on its own. The EEDF calculated from the line ratio method when using He-Ar was carried out using the ratio of Ar-811/Ar-750. There was a minimum EEDF value found when the Ar flow rate was set to $0.1 \, L \, min^{-1}$. Looking at Figure 10, the maximum value can be seen when the Ar flow rate is set to $0.5 \, L \, min^{-1}$ with a very little variance with changes in the applied voltage.

4 | DISCUSSION

As previously mentioned, the changes observed with respect to time were minimal and from which we can conclude that the plasma discharge was relatively stable and homogeneous throughout the system. Although there is a larger deviation in the emission of the N_2 SPS and OH, as seen in Figure 7, this is suspected to be due to variations in the populations of excited species as the suggested kinetic mechanisms take place. In order to determine the roots and mechanisms of excited N_2 generation and how Ar and He play roles, the emissions of atomic Ar and He need to be thoroughly analyzed. Before this can be done, however, an explanation must be found with regards to the interactions between the excited Ar and He species. This will provide a better understanding as to what steps and processes are most important for the generation of excited and reactive N_2 species. Looking through the results for each gas mixture, it can be seen that the highest intensity achieved is when a mixture of Ar-He with Ar being kept at a flow rate of $1 \, L \, min^{-1}$ and He of $0.1 \, L \, min^{-1}$ is used. This is even higher than just using Ar or He on its own at $1 \, L \, min^{-1}$. However, as He is increased to $0.5 \, L \, min^{-1}$ the intensity values of Ar in this gas mixture is comparable to when Ar is
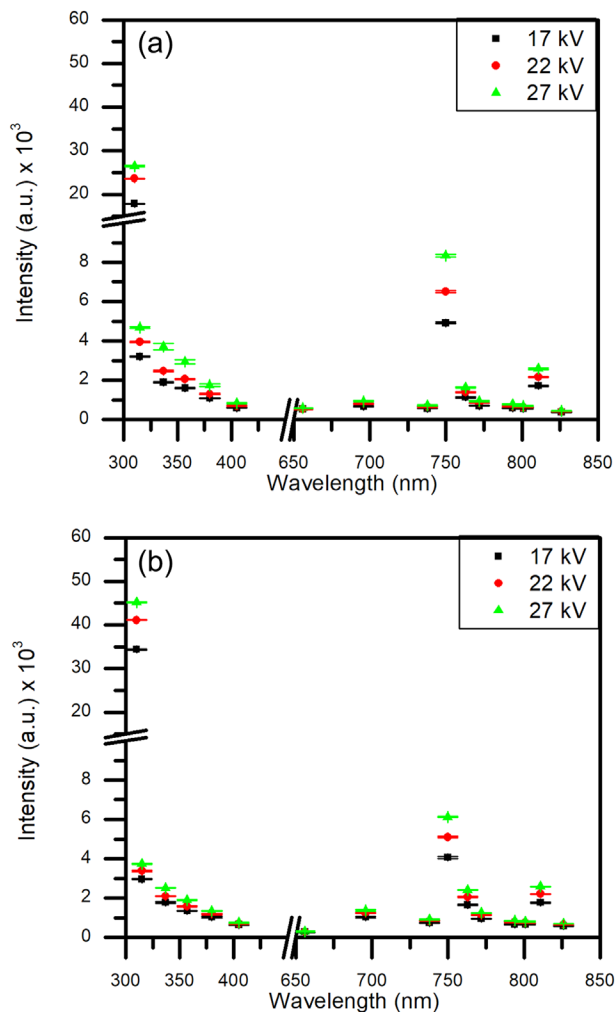
FIGURE 9 The changes in the intensities for the N_2 SPS, OH, Ar, and Hα are shown with the species being represented by their wavelength on the x-axis. The legend in 3(a) labels species (A-O) and the legend in Figure 5(a) labels species (P) that can be seen here. a) Shows the intensities when the flow rate of He-Ar is kept at 1 to 0.1 L min^{-1} and (b) represents intensities when He-Ar is kept at 1 to 0.5 L min^{-1}

FIGURE 10 The changes in the average EEDF obtained from the line ratio of Ar-811/Ar-750 when using He-Ar in air are shown. He is kept at 1 L min^{-1} the average EEDF is shown with respect to the positions along the plasma system when the flow rate of Ar = 0.1 L min^{-1} and Ar = 0.5 L min^{-1}.

the only gas used and kept at 1 L min^{-1}. It has been determined that the Ar species quench the energetic He atoms through Penning ionization. This means that there is a multi-step mechanism, similar to He-Ne discharge tubes, when using a mixture of Ar and He for plasma.

With this in mind, and noting how the resonant states of Ar are increased more so than the associated metastable emissions, there are two possible reasons for this apparent preferential pathway for energy transfer between He atoms and Ar atoms. For this we look at N_2, as the intensity of these excited species should also be affected by increases in metastable populations. The intensity of the excited N_2 species does in fact increase compared to when Ar is the sole gas, but is still less than for pure He, giving it the second highest values of intensity when using the Ar-He mix. The
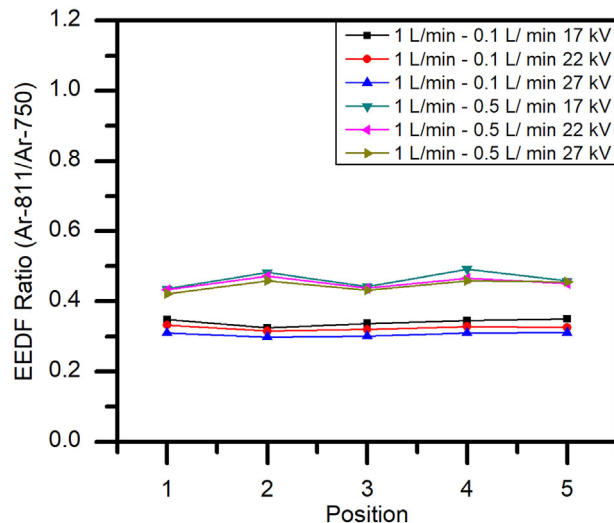
second, and most probable route for non-radiative energy transfer, is the interaction of He atoms with non-metastable resonant Ar species, such as the spectral emission at 696 nm. The reason that this is the likely route is that due to the much shorter lifetime of these species, the less likely the population will be saturated and a faster reaction time between these particles and He can occur. Going further than this, and basing other points on the experimental results obtained, the use of gas mixtures where Ar is the dominant gas (Ar-He) and where He is the dominant gas (He-Ar) show no detectable He emission lines or N_2^+-391. This would suggest that the He atoms are being quenched or are not excited to high enough states as when only He was used. Given that the Ar and N_2 SPS systems have increased intensities compared to when solely Ar was used, it would be suggested that the introduction of He creates a denser electron population to interact with N_2 and Ar. The lack of N_2^+-391 emission would suggest that the energies are not high enough to cause ionization. Looking at the N_2, Ar-811, and Ar-750 emission lines with changes of gas mixtures, credence can be given to the idea that He adds a larger amount of energetic electrons to the system and allows for a higher generation of N_2 SPS and Ar species. If the energy was high enough to ionize Ar, we would expect to also see some amount of N_2^+ as this can be created through Penning ionization with Ar$^+$, but given that none is detected, it is put forward that the main excitation kinetics for the Ar-750 and Ar-811 are due to electron interactions and allows us to use the line ratio method as was carried out for Ar alone. Taking into consideration both points, it is likely that both play a role in the energy transfer process, but the percentage
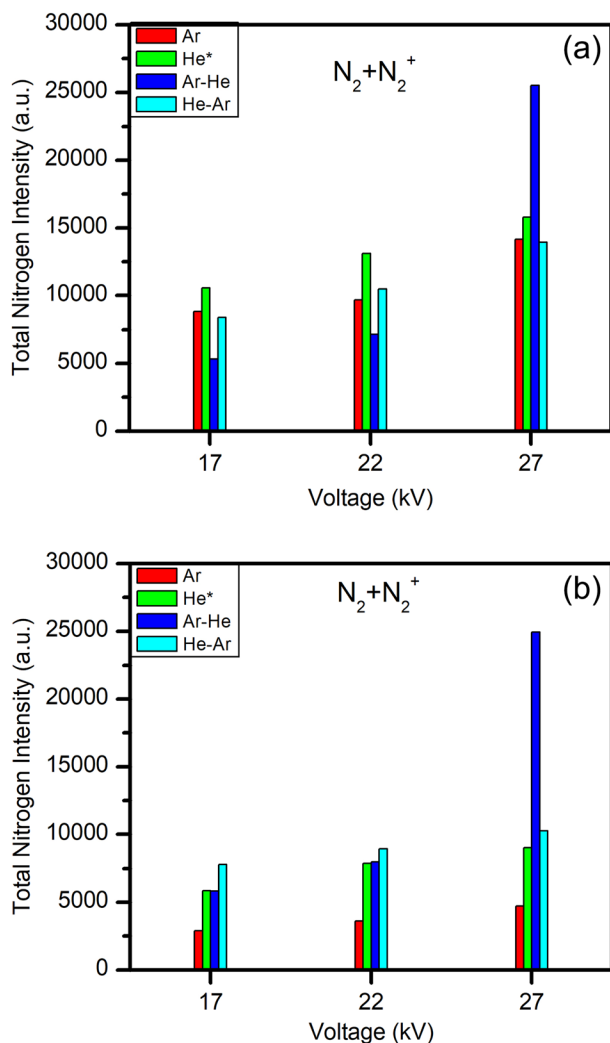
FIGURE 11 The total intensities for all nitrogen species generated during plasma discharge for each gas used during this study. a) Shows the intensities when the flow rate of Ar and He are at 1 L min^{-1} when used on their own and the mixtures of Ar-He and He-Ar were kept at 0.1 L min^{-1} and (b) shows the intensities when the flow rate of Ar and He are at 5 L min^{-1} when used on their own and the mixtures of Ar-He and He-Ar were kept at 0.5 L min^{-1}. (* N$_2^+$ was only recorded when He was used as the sole working gas for interactions with ambient air)

of interactions would be higher for those Ar species that are not metastables, and thus Penning excitation plays a major role in the kinetics of this work. As the gases were mixed, it was found that the intensity of the SPS was highest when the mixture of Ar-He was set to a ratio of 10:1 with a voltage of 27 kV PP. This can be seen in Figure 11(a,b).

However, it was found that there was no apparent emission of He when using the Ar-He mix, but He would obviously still be a contributing factor in the dynamics of the plasma kinetics and chemistry. As mentioned previously, the quenching of He due to the presence of Ar reduces the amount of He available to interact with N$_2$ and consequently when the quantity of Ar is larger than that of He, as seen with Ar-He, the emission lines are completely quenched and the energy is transferred from Ar to N$_2$. This can be supported by the fact that there was also no N$_2^+$ generated other than when using just He, thus showing that the high-energy atoms of He interact with Ar before having any chance of directly exciting N$_2$. This intermediary step of energy transfer to Ar and then to N$_2$ would decrease the efficiency of excited N$_2$ species as there would be energy loss when going from one species to another. Further, as the gas mixture of He-Ar is implemented, the intensity of excited N$_2$ species decreases due to the low amount of He available to interact with the entirety of the N$_2$ SPS due to quenching with Ar atoms, which also limits the maximum potential for energy transfer and again stops the generation of N$_2^+$. Finally, by using Ar on its own, there is a limit to the maximum intensity as the excitation comes directly from the power supplied to the system which, by extension, limits the amount of excited N$_2$ species generated as there is less possibility of energy transfer through collisions with higher energy particles such as He atoms. From this, there is a benefit to utilize an addition of He to generate a potential non-radiative collisional transfer of energy with Ar when a ratio is maintained with He being roughly 10 times less than Ar. Table 4 shows the factor differences of total nitrogen emissions for each gas and gas mixture used.

TABLE 4 Factor differences between the total nitrogen emissions when comparing the intensities of the Ar-He mixture to the other gases used to highlight the effect of optimizing the selectivity process (i.e., [Ar-He intensity/compared gas intensity])

	Flow rate			Flow rate		
	1 L min^{-1}		**0.1 L min^{-1}**	**5 L min^{-1}**		**0.5 L min^{-1}**
Voltage/gas	**Ar**	**He**	**He-Ar**	**Ar**	**He**	**He-Ar**
17 kV	0.603	0.503	0.634	2.012	0.996	0.750
22 kV	0.739	0.546	0.683	2.220	1.013	0.891
27 kV	1.801	1.614	1.831	5.283	2.760	2.429

5 | CONCLUSION

It has been found that the use of Ar, He, and mixes of these gases is a viable method for enhanced selectivity of excited N_2 species generation at a lower voltages, current, and temperatures compared to using solely ambient air. By using Ar, there were strong signals of the N_2 SPS and when using He the highest values for the intensity of the N_2 SPS and FNS were recorded. It was also found that by mixing the gases together that interactions occur between the Ar and He atoms present causing the He species to be quenched. Similar findings can be found in the electrical discharges of helium and neon mixes. Although there was no atomic oxygen detected in the plasmas generated in this work, ozone is likely generated. This could possibly be the reason why there was no detection of NO emissions during plasma discharge, with any atomic oxygen sufficiently excited to bond to O_2 and create O_3, thus eliminating interactions with atomic nitrogen. Biological studies using this reactor (not a part of this work) showed a reduction in bacteria activities due to the O_3 molecule. Overall, it was found that the optimum parameter used to generate the most amount of N_2 excited species for interaction with samples was when He was used, but the gas mixture of Ar-He with Ar at $1 \, \text{L} \, \text{min}^{-1}$ and He at $0.5 \, \text{L} \, \text{min}^{-1}$ was capable of creating a relatively high intensity of N_2 while minimizing the amount of He and Ar present for interactions.

ORCID

Laurence Scally (iD) http://orcid.org/0000-0002-3246-725X
Patrick J. Cullen (iD) http://orcid.org/0000-0001-7654-6171
Vladimir Milosavljević (iD) http://orcid.org/0000-0002-7805-5189

REFERENCES

[1] E. E. Kunhardt, *IEEE Trans. Plasma Sci.* **2000**, *28*, 189.
[2] A. P. Napartovich, *Plasmas Polym.* **2001**, *6*, 1.
[3] R. Ono, T. Oda, *Int. J. Plasma Environ. Sci. Technol.* **2007**, *1*, 123.
[4] D. L. Crintea, U. Czarnetzki, S. Iordanova, I. Koleva, D. Luggenhölscher, *J. Phys. D: Appl. Phys.* **2009**, *42*, 045208.
[5] D. Xiao, C. Cheng, J. Shen, Y. Lan, H. Xie, X. Shu, Y. Meng, J. Li, P. K. Chu, *J. Appl. Phys.* **2014**, *115*, 033303.
[6] M. Thiyagarajan, A. Sarani, C. Nicula, *J. Appl. Phys.* **2013**, *113*, 233302.
[7] Z. B. Wang, G. X. Chen, Z. Wang, N. Ge, H. P. Li, *J. Appl. Phys.* **2011**, *110*, 033308.
[8] K. D. Weltmann, T. von Woedtke, *Plasma Phys. Control. Fusion* **2016**, *59*, 014031.
[9] Y. K. Jo, J. Cho, T. C. Tsai, D. Staack, M. H. Kang, J. H. Roh, D. B. Shin, W. Cromwell, D. Gross, *Crop Sci.* **2014**, *54*, 796.
[10] C. Heslin, D. Boehm, V. Milosavljević, M. Laycock, P. J. Cullen, P. Bourke, *Plasma Med.* **2014**, *4*, 153.
[11] G. Fridman, G. Friedman, A. Gutsol, A. B. Shekhter, V. N. Vasilets, A. Fridman, *Plasma Process. Poly.* **2008**, *5*, 6.
[12] L. Scally, J. Lalor, P. J. Cullen, V. Milosavljević, *J. Vac. Sci. Tech. A: Vac. Surf. Films* **2017**, *35*, 105.
[13] V. Cristaudo, S. Collette, N. Tuccitto, C. Poleunis, L. C. Melchiorre, A. Licciardello, F. Reniers, A. Delcorte, *Plasma Process. Polym.* **2016**, *13*, 11.
[14] S. K. Øiseth, A. Krozer, B. Kasemo, J. Lausmaa, *Appl. Surf. Sci.* **2002**, *202*, 92.
[15] G. Daeschlein, T. von Woedtke, E. Kindel, R. Brandenburg, K.-D. Weltmann, M. Jünger, *Plasma Process. Polym.* **2009**, *7*, 3–4.
[16] Q. S. Yu, H. Li, A. C. Ritts, B. Yang, M. Chen, L. Hong, C. Xu, X. Yao, Y. Wang, *Plasma for Bio-Decontamination, Medicine and Food Security*, NATO Science, Springer, Dordrecht **2012**.
[17] C. W. Liu, Y. Sung, B. C. Chen, H. Y. Lai, *Intern. J. Environ. Res. Pub. Health* **2014**, *11*, 4427.
[18] M. A. Lloyd, S. J. Hess, M. A. Drake, *J. Dairy Sci.* **2009**, *92*, 2409.
[19] E. Marasca, D. Greetham, S. D. Herring, I. D. Fisk, *Food Chem.* **2016**, *199*, 81.
[20] A. S. Silva, J. L. Hernández, P. P. Losada, *Analy. Chem. Acta* **2004**, *524*, 185.
[21] N. Morgan, D. Ibrahim, A. Samir, *J. Ener. Environ. Chem. Eng.* **2017**, *2*, 25.
[22] M. Penetrante, R. M. Brusasco, B. T. Merritt, G. E. Vogtlin, *Plasmas Pure App. Chem.* **1999**, *71*, 1829.
[23] B. M. Penetrante, M. C. Hsiao, J. N. Bardsley, B. T. Merritt, G. E. Vogtlin, A. Kuthi, C. P. Burkhart, J. R. Bayless, *Plasma Sources Sci. Technol.* **1997**, *6*, 251.
[24] J. V. Durme, J. Dewulf, C. Leys, H. V. Langenhove, *Appl. Catal. B: Environ.* **2008**, *78*, 324.
[25] X. Lu, G. V. Naidis, M. Laroussi, S. Reuter, D. B. Graves, K. Ostrikov, *Phys. Rep.* **2016**, *630*, 1.
[26] M. Ishaq, M. Evans, K. Ostrikov, *Int. J. Can.* **2013**, *134*, 1517.
[27] F. Liu, P. Sun, N. Bai, Y. Tian, H. Zhou, S. Wei, Y. Zhou, J. Zhang, W. Zhu, K. Becker, J. Fang, *Plasma Process. Polym.* **2009**, *7*, 3–4.
[28] M. Janda, V. Martišovitš, K. Hensel, Z. Machala, *Plasma Chem. Plasma Process.* **2016**, *36*, 767.
[29] M. J. Traylor, M. J. Pavlovich, S. Karmin, P. Hait, Y. Sakiyama, D. S. Clark, D. B. Graves, *J. Phys. D: Appl. Phys.* **2001**, *44*, 472001.
[30] B. K. H. L. Boekema, M. Vlig, D. Guijt, K. Hijnen, S. Hofmann, P. Smits, A. Sobota, E. M. van Veldhuizen, P. Bruggeman, E. Middelkoop, *Phys. D: Appl. Phys.* **2015**, *49*, 044001.
[31] A. Kramida, Y. Ralchenko, J. Reader, NIST ASD Team. **2015**. NIST Atomic Spectra Database (ver. 5.3), [Online]. Available: http://physics.nist.gov/asd [2017, September 29]. National Institute of Standards and Technology, Gaithersburg, MD.
[32] V. Milosavljević, M. Donegan, P. J. Cullen, D. P. Dowling, *J. Phys. Soc. Jap.* **2014**, *83*, 014501.
[33] D. Hegemann, H. Brunner, C. Oehr, *Nuc. Instr. Meth. Phys. Res. Sec. B* **2003**, *208*, 281.

[34] H. H. Richter, A. Wolff, R. Hippler, S. Pfau, M. Schmidt, K. H. Schoenbach (Eds), *Low Temperature Plasma Physics*, Wiley-VCH, Berlin **2001**.

[35] J. P. Youngblood, T. J. McCarthy, *Macromolecules* **1999**, *32*, 6800.

[36] J. W. Coburn, H. F. Winters, *J Appl. Phys.* **1979**, *50*, 3189.

[37] I. P. Herman, *Optical Diagnostics for Thin Film Processing* (1st ed.), Academic Press, Cambridge, MA **1995**.

[38] R. Friedl, U. Fantz, *New J. Phys.* **2012**, *14*, 043016.

[39] V. Milosavljević, P. J. Cullen, *Euro. Lett.* **2015**, *110*, 43001.

[40] J. B. Boffard, R. O. Jung, C. C. Lin, A. E. Wendt, *Plasma Sources Sci. Technol.* **2010**, *19*, 065001.

[41] I. A. Biloiu, E. E. Scime, *Phys. Plasmas* **2010**, *17*, 113508.

[42] V. M. Donnelly, *J. Phys. D: Appl. Phys.* **2004**, *37*, R207–R236.

[43] J. B. Boffard, G. A. Piech, M. F. Gehrke, L. W. Anderson, C. C. Lin, *Phys. Rev. A* **1999**, *59*, 1050–2947.

[44] M. A. Naveed, A. Qayyum, S. Ali, M. Zakaullah, *Phys. Lett. A* **2006**, *359*, 499–503.

[45] A. Begum, M. Laroussi, M. R. Pervez, *AIP Adv.* **2013**, *3*, 062117.

[46] V. Milosavljević, P. J. Cullen, *Euro. Phys. J. Appl. Phys.* **2017**, *80*, 20801.

[47] A. Schmidt-Bleker, J. Winter, A. Bösel, S. Reuter, K.-D. Weltman, *Plasma Sources Sci. Technol.* **2016**, *25*, 015005.

[48] J. Jánsky, A. Bourdon, *Plasma Sources Sci. Technol.* **2014**, *23*, 025001.

[49] A. R. Hoskinson, J. Gregorío, J. Hopwood, K. Galbally-Kinney, S. J. Davis, W. T. Rawlins, *J. Appl. Phys.* **2016**, *119*, 233301.

[50] J. K. Olthoff, R. J. Van Brunt, S. B. Radovanov, J. A. Rees, *IEE Proc. Sci. Meas. Technol.* **1994**, *141*, 1350–2344.